Remarks:

Claims 1-29 are pending in the subject application. Claims 23-29 are withdrawn. Claims 1-22 stand rejected. Claims 18 and 19 are amended herein to correct minor typographical errors. The amendments herein are fully supported by the Subject Application as filed and do not add new matter to the Subject Application

The Rejections

The Rejections Under 35 U.S.C. §103(a)

Claims 1-22 stand rejected under 35 U.S.C. § 103(a) as having been obvious over U.S. Patent No. 4,956,012 to Jacobs et al. ("Jacobs"). Applicant traverses this rejection for the reasons set forth herein.

Establishing a *prima facie* case of obviousness under §103(a) requires that the cited reference or references teach or suggest every element and limitation recited in the rejected claim. *See, e.g.,* MPEP § 2142. In the present case, and as discussed below, the Examiner has not established a *prima facie* case that the rejected claims would have been obvious for at least the reason that Jacobs does not teach or suggest each and every element and limitation of rejected independent claims 1 and 15.

In the Office Action, the Examiner rejects claims 1-22 as have been obvious over Jacobs because "Jacobs Figure 4 suggests that these [embodiments of Jacobs] include embodiments possessing the features presently claimed." Further, the Examiner states that "... it is noted that Applicant states in paragraph [0010] of the present specification that at least one embodiment of the Jacobs patent has a contiguity ratio of about 0.52, which would be outside the range as defined in instant claim 1. However, it is unclear how Applicant arrived at such a calculation."

The contiguity ratio of 0.52 referred to in paragraph [0010] of the Subject Application was calculated based on Figure 2 in the Subject Application, which is identical to Figure 3 in Jacobs. The method used to calculate the contiguity ratio can be found in J. Gurland, "Application of Quantitative Microscopy to Cemented Carbides", Practical Applications of Quantitative Metallography, ASTM Special Technical

Publication 839, pp. 65, 70-76 (ASTM 1984). Gurland applied the concept of a contiguity ratio to cemented carbides. The more general metallographic concept of a contiguity ratio, however, initially was described in part by E.E. Underwood in Underwood, Quantitative Stereology, pp. 279-290 (Addison Wesley, 1970), which is cited in paragraph [0027] of the Subject Application. Applicant attaches the relevant portions of Gurland to this Response. Applicant also attaches a declaration by Dr. Prakash Mirchandani ("the Declaration"), the inventor named on the Subject Application, describing how the contiguity ratio of a hybrid cemented carbide is calculated, and setting out in detail how the contiguity ratio for Figures 2 and 4A of the Subject Application is calculated.

As generally discussed in the Declaration, the contiguity ratio is a value describing a physical characteristic of something including two phases. In other words, two phases must be present in order to determine a contiguity ratio. Gurland applies the general metallographic concept of contiguity ratio to cemented carbides, which are materials including a dispersed, discontinuous, hard phase and a continuous phase of binder. Dr. Mirchandani applies the concept of contiguity ratio to hybrid cemented carbides, which also include at least two phases in the form of a dispersed, discontinuous phase of cemented carbide and a continuous, binder phase of cemented carbide. (Of course, in a hybrid cemented carbide each individual cemented carbide phase, both the discontinuous and the continuous phases, includes both a discontinuous and a continuous phase, but this fact is irrelevant to the calculation of a contiguity ratio for the hybrid cemented carbide overall.)

Figure 2 of the Subject Application (which is the same as Figure 3 of Jacobs) is an embodiment of Jacobs shown at 100X magnification. Figure 2 shows a darker-colored discontinuous phase of cemented carbide within a lighter-colored continuous phase of cemented carbide. As discussed above, these are the two relevant phases for calculating the contiguity ratio of the hybrid cemented carbide. In the Declaration, Dr. Mirchandani describes how the method of Gurland is applied to Figure 2 of the Subject Application, resulting in a contiguity ratio of 0.53, which is outside the range of claim 1.

Figure 4 of Jacobs is a photograph of the same embodiment shown in Jacob's Figure 3, but is at 1500X magnification, which is 15 times the magnification of Jacob's Figure 3. Because of the extreme magnification shown in Jacob's Figure 4, all that can be seen in the figure is the darker-colored discontinuous phase. Because the other phase relevant to determining contiguity ratio (*i.e.*, the lighter-colored continuous phase) is not visible in Jacob's Figure 4, one cannot calculate a contiguity ratio from that figure. Nevertheless, Jacob's Figure 4 depicts the same composite as shown in the patent's Figure 3, which has a contiguity ratio of 0.53. A contiguity ratio of 0.53 falls outside the range recited in claim 1 of the Subject Application.

Dr. Mirchandani's declaration also describes how the method of Gurland is applied to determine a contiguity ratio from Figure 4B of the Subject Application. Figure 4B is an embodiment of the invention of the Subject application, and in the Declaration Dr. Mirchandani calculates a contiguity ratio of 0.32 from the figure, which is within the range of claim 1 of the Subject Application.

Therefore, as discussed above and as shown in the attached Declaration, Jacobs does not disclose, either expressly or inherently, a hybrid cemented carbide wherein the contiguity ratio of the dispersed, discontinuous phase is less than or equal to 0.48, as recited in claim 1. Jacobs also does not disclose, either expressly or inherently, a hybrid cemented carbide wherein the dispersed phase has a contiguity ratio less than or equal to 1.5 times the volume fraction of the dispersed phase in the composite, as recited in claim 15. Therefore, the Examiner has not established a *prima facie* case of obviousness for at least the reason that Jacobs does not teach or suggest each and every element and limitation of rejected independent claims 1 and 15. Thus, Applicant respectfully requests withdrawal of the rejection of claims 1-22 and subsequent allowance of those claims.

The Nonstatutory Obviousness-Type Double Patenting Rejection

Although Applicant respectfully disagrees with the Examiner's allegation that the inventions recited in the Subject Application and in co-pending application Serial Nos. 11/013,842 and 11/167,811 are not patentably distinct, Applicant chooses not to address the rejection at this time. The Subject Application has the earliest filing date of

the three co-pending applications. Pursuant to MPEP § 804 and other sections of the MPEP, it is proper to ignore an obviousness-type double patenting ("ODP") rejection in the earlier-filed application. As explained in the MPEP, if the ODP rejection is the last rejection remaining in the earlier-filed application, the examiner should withdraw the ODP rejection and allow the earlier-filed application to issue, without need for the Applicant to submit a terminal disclaimer. With this understanding, and with the understanding that Applicant reserves the right to argue against the ODP rejection in the later-filed applications, Applicant chooses not to address the ODP rejection in the Subject Application.

Conclusion:

Applicant respectfully submits that the claims of the Subject Application, as amended herein, are directed to subject matter that is patentable over the cited references. Applicant respectfully requests issuance of a Notice of Allowance at an early date. If, however, the Examiner is of the opinion that the Subject Application is in condition for disposition other than allowance, Applicant respectfully requests that the Examiner contact Applicant's attorney at the telephone number listed below so that those concerns may be addressed.

Respectfully submitted,

Mark R. Leslie, Esq.
Registration No. 36,360
Attorney for Applicant

KIRKPATRICK & LOCKHART PRESTON GATES ELLIS LLP
Henry W. Oliver Building
535 Smithfield Street
Pittsburgh, Pennsylvania 15222-2312
Phone: 412.355.6271

Practical Applications of Quantitative Metallography

McCall/Steele, editors

PRACTICAL APPLICATIONS OF QUANTITATIVE METALLOGRAPHY

A symposium sponsored by
ASTM Committee E-4 on
Metallography and by the
International Metallographic Society
Orlando, Fla., 18–19 July 1982

ASTM SPECIAL TECHNICAL PUBLICATION 839
J. L. McCall, Battelle Columbus Laboratories,
and J. H. Steele, Jr., Armco Inc.,
editors

ASTM Publication Code Number (PCN)
04-839000-28

1916 Race Street, Philadelphia, Pa. 19103

International Metallographic Society

Library of Congress Catalog Card Number: 83-73230

NOTE

The Society is not responsible, as a body,
for the statements and opinions
advanced in this publication.

Printed in Ann Arbor, Mich.
July 1984

Joseph Gurland[1]

Application of Quantitative Microscopy to Cemented Carbides

REFERENCE: Gurland, J., "**Application of Quantitative Microscopy to Cemented Carbides,**" *Practical Applications of Quantitative Metallography, ASTM STP 839*, J. L. McCall and J. H. Steele, Jr., Eds., American Society for Testing and Materials, Philadelphia, 1984, pp. 65–84.

ABSTRACT: Among the cemented carbides, the tungsten carbide/cobalt (WC-Co) alloys are the most studied. Four parameters are used to characterize their microstructures: the binder volume fraction, binder mean free path, carbide grain size, and carbide contiguity. Some success has been achieved in relating these variables empirically and theoretically to mechanical properties relevant to performance, such as hardness and toughness. Current research is directed towards the possibly significant effects of the fine substructures—specifically, those of solutes, precipitates, stacking faults, and other defects in the binder—and those of the binder metal concentration and dislocation arrays at the grain boundaries of the tungsten carbide.

This review briefly describes the use of microscopy in quality evaluation, microstructural characterization, and alloy development.

KEY WORDS: quantitative metallography, cemented carbides, tungsten carbide/cobalt alloy, stereology, quantitative microscopy, quality evaluation

Commercial cemented carbide grades generally consist of two constituents: the carbide [tungsten carbide (WC), titanium carbide (TiC), tantalum carbide (TaC), vanadium carbide (VC), niobium carbide (NbC), and so forth, and their solid solutions] and the binder (cobalt, nickel, or iron, with or without additives and containing dissolved elements of the carbide). In principle, their simple microstructures, consisting of chemically and physically well-defined phases, lend themselves to quantitative characterization, and, in fact, light microscopy and electron microscopy are widely used in production control, quality evaluation, and alloy development. The basic methods of microscopic evaluation of cemented carbides merit their own ASTM and International Organization for Standardization (ISO) standards, and active international interaction is taking place to refine and expand the scope of these methods.

[1] Professor of engineering, Division of Engineering, Brown University, Providence, R.I. 02912.

The application of microscopic methods to interpretation of the microstructure of cemented carbides has been reviewed from time to time, most recently by Exner [*1*][2] and Cherniavsky [*2*]. The present review will first describe the use of standard stereological concepts for quality control and alloy development and then briefly discuss and illustrate some of the less common approaches and methods used for research purposes.

Qualitative Comparative Examination for Quality Evaluation

The user of carbide tools might start by examining the fracture surface of a piece of questionable quality: the piece would have been either broken in use, crushed for the purpose by a hammer blow, or broken in a fracture test. Inspection through a low-power lens (×15 to ×40) often reveals qualitative evidence of porosity, excess carbon, and contamination. A very smooth fracture surface, with a characteristic "river" pattern, indicates cleavage and, generally, brittleness [Fig. 1 (*top*)]. Often the large pores and other defects from which the fracture started can be detected. The degree of brittleness to be expected depends, of course, on the grade or alloy. A tougher piece or grade has a dull, satiny, or rough surface associated with greater fracture resistance [Fig. 1 (*bottom*)].

The next step usually is the metallographic determination of the apparent porosity by low-power light microscopy [ASTM Test for Apparent Porosity in Cemented Carbides (B 276-79)]. The surface preparation consists of grinding and polishing a flat section with successively finer diamond powder or paste, finishing with diamond grit of 3-μm particle size. The term apparent porosity refers to the microstructure, observed on the polished but unetched surface and associated not only with the true inherent porosity but also with uncombined carbon and foreign inclusions, all of which generally appear as dark specks on the shiny background of the polished metallic surface (Fig. 2). The pattern of the apparent porosity is compared visually with the photomicrographs of the ASTM standard at a specified magnification of ×100 or ×200 and is classified as to type (porosity or uncombined carbon), size of pores, and area fraction of pores. Good-quality commercial products are generally found to be at the low end of the porosity scale.

Determination of the apparent porosity is often teamed with measurements of the density (ASTM Test for Density of Cemented Carbides [B 311-58(1979)], hardness (ASTM Hardness Testing of Cemented Carbides [B 294-76(1982)]), and transverse rupture strength (ASTM Test for Transverse Rupture Strength of Cemented Carbides [B 406-76(1982)]) to provide the basic "first echelon" input for quality evaluation.

For the purposes of alloy identification and defect characterization, the actual microstructure is examined at higher magnification, typically at ×1500,

[2]The italic numbers in brackets refer to the list of references appended to this paper.

in the light microscope (Fig. 3). The ASTM Method for Metallographic Determination of Microstructure in Cemented Carbides (B 657-79) provides instructions for surface preparation and etching procedures. The standard etching solutions are Murikami's reagent [a mixture of equal amounts of 10% aqueous solution of potassium ferricyanide ($K_3Fe(CN)_6$) and potassium or sodium hydroxide] and dilute hydrochloric acid. The various phases are labeled as follows: tungsten carbide (α phase), binder metal (β phase), and cubic carbides, TiC, TaC, NbC, and other carbides, individually or as mixed carbides in solution (γ phase). Also looked for is the presence of free carbon in the microstructures of high-carbon alloys or of the η-type phase (eta), an intermetallic compound of carbides and binder metal typically found in carbon-deficient materials (Fig. 4) [*3*]. The presence of the η phase in appreciable amounts is always deleterious and indicates low fracture strength. Carbide grain sizes are evaluated by ASTM Method B 657-79 and the ASTM Recommended Practice for Evaluating Apparent Grain Size and Distribution of Cemented Tungsten Carbides [B 390-64(1982)].

The visual identification of the constituents is sometimes supplemented by X-ray diffraction and X-ray fluorescence analysis. Also at this stage of quality evaluation, additional physical properties are commonly measured, namely, coercive force and magnetic saturation, which give indications of the amount and distribution of the binder, the carbon content of the binder, and, indirectly, the grain size and grain size distribution of the carbide phase. The total carbon content and the amount of free, uncombined carbon are also determined by chemical analysis.

Stereological Methods for the Quantitative Characterization of Microstructures for Alloy Development

In order to correlate mechanical properties with microstructural parameters, the latter need to be established quantitatively and precisely. What feature or, more likely, what combination of features controls specific properties or performance is still a matter of controversy, but there is general agreement that the alloy composition, carbide grain size, and binder ligament width are of primary practical relevance.

Because of the fine dispersion of carbide and binder in cemented carbides, the resolution of the light microscope is often insufficient, and electron microscopy is required for accurate and precise measurements of volume fractions and sizes. In electron microscopy, the older surface replica method [*4*] has been replaced by scanning electron microscopy with backscattered electrons or secondary electron emission. Various chemical and electrolytic etching procedures are described in the literature [*5*] but, generally, the same etching solutions can be used as for light microscopy (Fig. 5).

By alloy composition is meant the volume fractions of the constituents, that is, the carbide and binder phases. ASTM provides the recommended practice

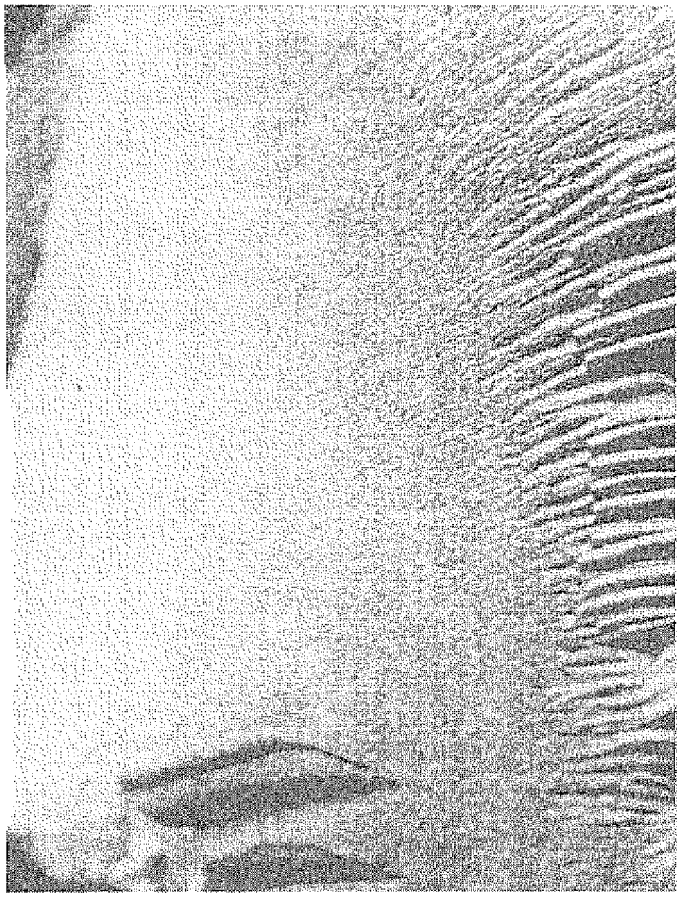

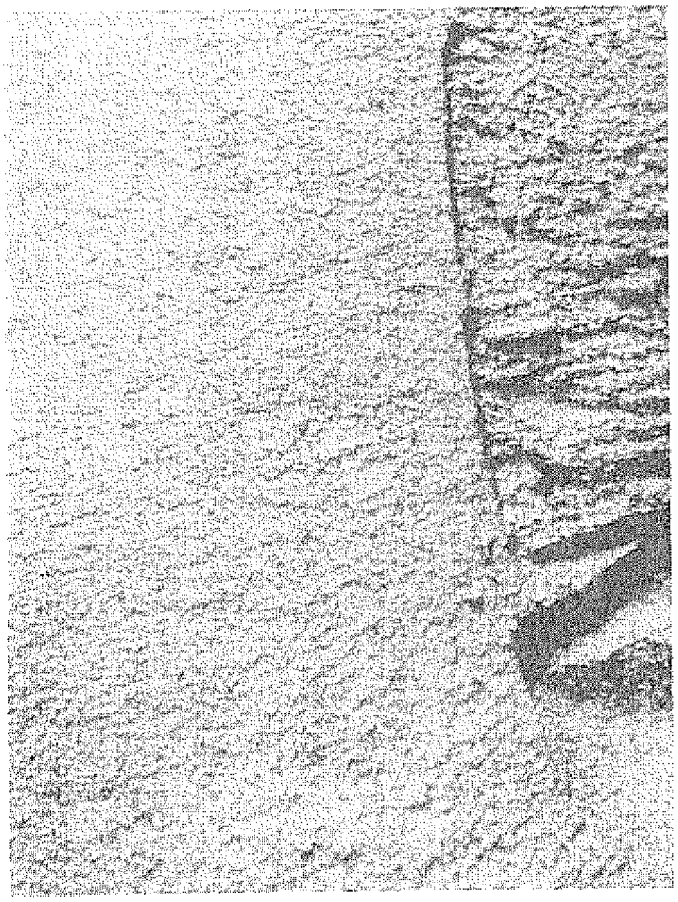

FIG. 1—*Fracture surfaces of commercial grades of WC-Co at ×40: (top) 6% cobalt by weight, (bottom) 16% cobalt by weight.*

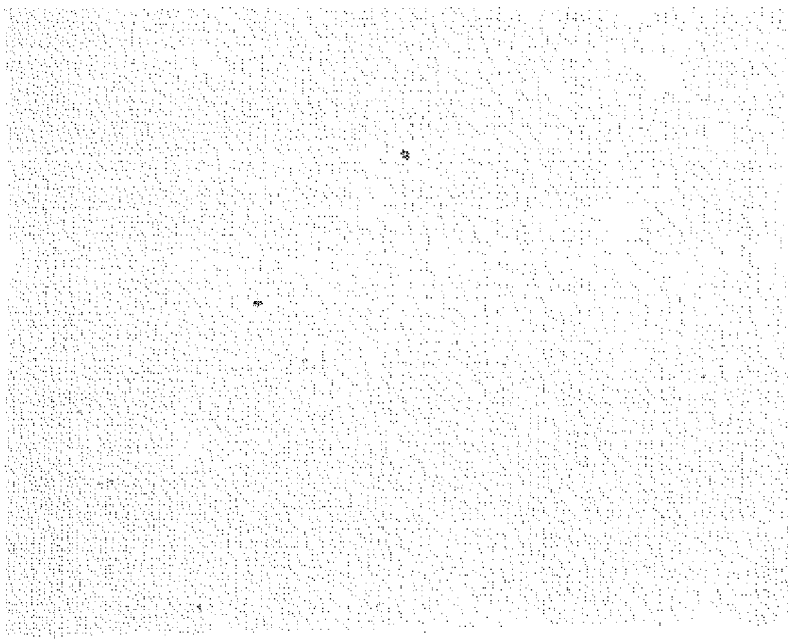

FIG. 2—*Typical porosity of commercial grade WC-Co, unetched surface,* ×200.

for estimation of the area fraction of a phase in a multiphase alloy by systematic point counting on a planar test section [ASTM Recommended Practice for Determining Volume Fraction by Systematic Manual Point Count (E 562-76)] (Fig. 6). The point fraction, $(P_P)_\alpha$, intercepted by the α phase, statistically interpreted, provides an estimate of the volume fraction, $(V_V)_\alpha$, area fraction, $(A_A)_\alpha$, and line fraction, $(L_L)_\alpha$. For statistically random microstructures or statistically random measurements

$$(P_P)_\alpha = (L_L)_\alpha = (A_A)_\alpha = (V_V)_\alpha \tag{1}$$

Further structural information is obtained from boundary intercepts with test lines on planar sections. The test lines might be the lines of a transparent grid superimposed upon the microstructure. In the case of tungsten carbide/cobalt (WC-Co) alloys, for instance, one determines the average number of intercepts per unit length of test line with traces of the carbide/cobalt interface, $(N_L)_{\alpha\beta}$, and carbide/carbide grain boundaries, $(N_L)_{\alpha\alpha}$, respectively (Fig. 6). The following parameters can then be calculated:

1. The tungsten carbide mean linear intercept grain size

$$(\bar{L}_3)_\alpha = \frac{2(V_V)_\alpha}{2(N_L)_{\alpha\alpha} + (N_L)_{\alpha\beta}} \tag{2}$$

where $(V_V)_\alpha$ is the volume fraction of the carbide phase.

2. The contiguity of tungsten carbide

$$C_\alpha = \frac{2(N_L)_{\alpha\alpha}}{2(N_L)_{\alpha\alpha} + (N_L)_{\alpha\beta}} \tag{3}$$

3. The binder mean linear intercept distance, that is, the mean free path

$$\bar{L}_\beta = \frac{2(V_V)_\beta}{(N_L)_{\alpha\beta}} \tag{4}$$

where $(V_V)_\beta$ is the volume fraction of the binder phase. Similar measurements can be carried out on the cubic carbides (γ phase), if present.

The mean linear intercept grain size of WC is identical with the mean carbide particle size. It is the particle intercept length averaged over all directions

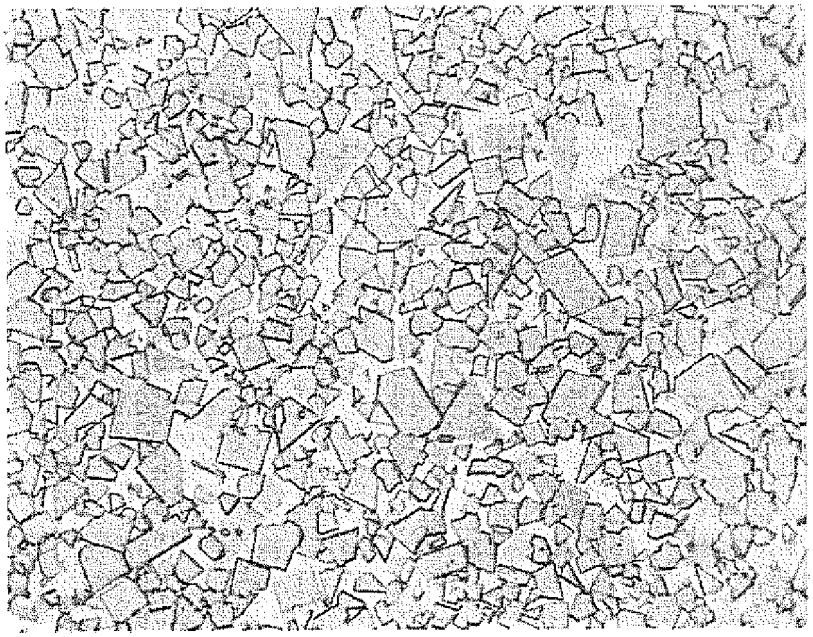

FIG. 3—*Microstructure of commercial grade WC, 16% cobalt by weight, etched with Murikami's reagent, light microscope photomicrograph, ×1500.*

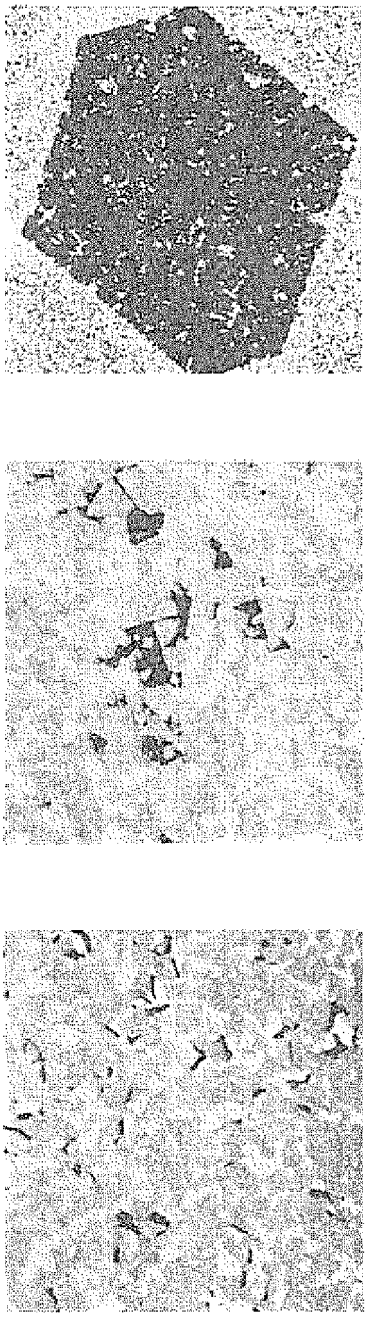

FIG. 4—*Graphite and η phase in WC-Co [3]: (left) graphite in a carbon-rich specimen, 16% cobalt, unetched, ×1500; (middle) η phase in a carbon-deficient specimen, 16% cobalt, etched 10 s with Murikami's reagent, ×1500; (right) abnormally large η phase gram resulting from long-time decarburization, ×125.*

and all particles. It is directly related to the total surface area of the carbide grains per unit volume, $(S_V)_\alpha$, since

$$(S_V)_\alpha = \frac{4(V_V)_\alpha}{(L_3)_\alpha} \tag{5}$$

where $(S_V)_\alpha$ includes the tungsten carbide (WC)/cobalt interfaces and WC/WC grain boundaries. The mean free path in the binder is a measure of the average thickness of the binder layers and also of the total area of the WC/cobalt interface per unit volume

$$(S_V)_\beta = \frac{4(V_V)_\beta}{\bar{L}_\beta} \tag{6}$$

The grain boundaries of the binder are ignored in these calculations since, in general, the grain size of the binder is very much larger than the mean free path between carbide particles. The contiguity is a measure of the degree of contact between carbide particles. It is defined as the ratio of the WC/WC grain boundary area to the total surface area of the carbide, the latter consisting of WC/WC grain boundaries and WC/cobalt interfaces.

The evaluation of these basic stereological parameters is independent of shape and size, but the structure parameters discussed so far are not independent of each other, as shown by their interrelation

$$\bar{L}_\beta = (\bar{L}_3)_\alpha \frac{(V_V)_\beta}{[1-(V_V)_\beta]\,(1-C_\alpha)} \tag{7}$$

According to Eq 7, any three of the four parameters are sufficient to characterize fully the degree of dispersion of the carbide phase in WC-Co alloys. The theories and practices relevant to these stereological parameters are discussed in detail by Underwood [*6*].

Considerable effort has been expended in attempting to replace the tedious manual point and intercept counting by automatic scanning procedures. Not only can these give the average values of the parameters quickly and easily, but they also lend themselves to further exploitation of the accumulated data, specifically, by supplying information on size distribution, shape factors, and orientation. Unfortunately, the required gray-level distinction is particularly difficult to achieve in cemented carbides because of the fineness of the structure and poor contrast between phases. While automatic methods have not yet generally established themselves in the industry, two interesting approaches are worth mentioning. Nidikom and Davies [*7*] used a special double-etching procedure to increase the contrast between binder and carbide in WC-Co sufficiently to allow scanning by an image analyzing computer. Werlefors and

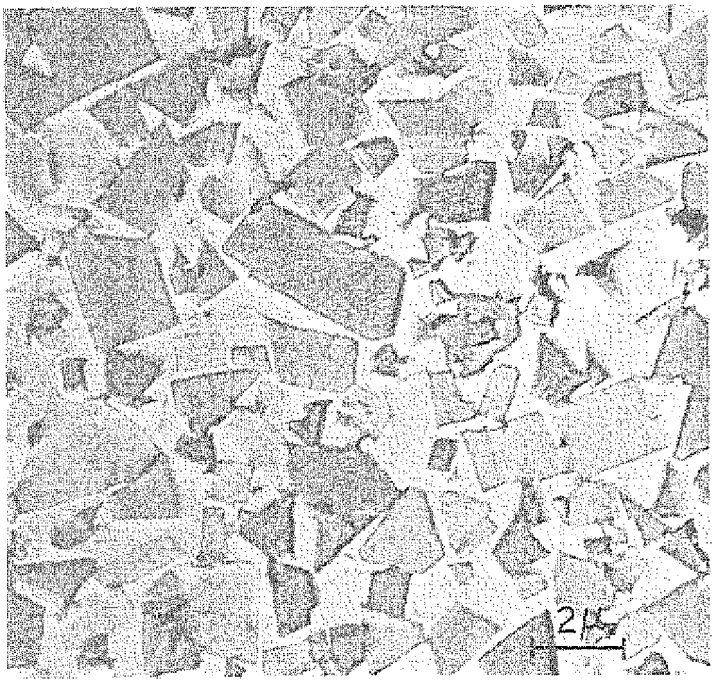

FIG. 5—*Electron photomicrographs of WC-Co, electrolytic etch, replica TEM [10]:* (a) *15% cobalt by weight.*

Eskilsson [*8*] supplemented on-line computer analysis of electron microscope scans by interactive manual tracing of WC/WC grain boundaries by the operator. Other semiautomatic devices, requiring hand tracing of the grain and interphase boundaries on an electronic planimeter (digitizer tablet), with on-line data storage and analysis by computer, are commercially available. Their application to cemented carbides is described by Exner [*1*].

The empirical effects on properties of the aforementioned parameters are well established. High porosity affects density, of course, but even very low porosity may influence fracture strength in a way that is out of proportion to its amount because of the role of critically sized or critically spaced flaws in fracture nucleation.

The overall effects of the cobalt content and WC grain size on the hardness, transverse rupture strength, and fracture toughness are perhaps best summarized by showing the variation in these properties as a function of the binder mean free path (Fig. 7). In general, the hardness decreases and the fracture toughness increases with an increasing mean free path, that is, with increasing cobalt content or increasing WC grain size. The shape of the transverse

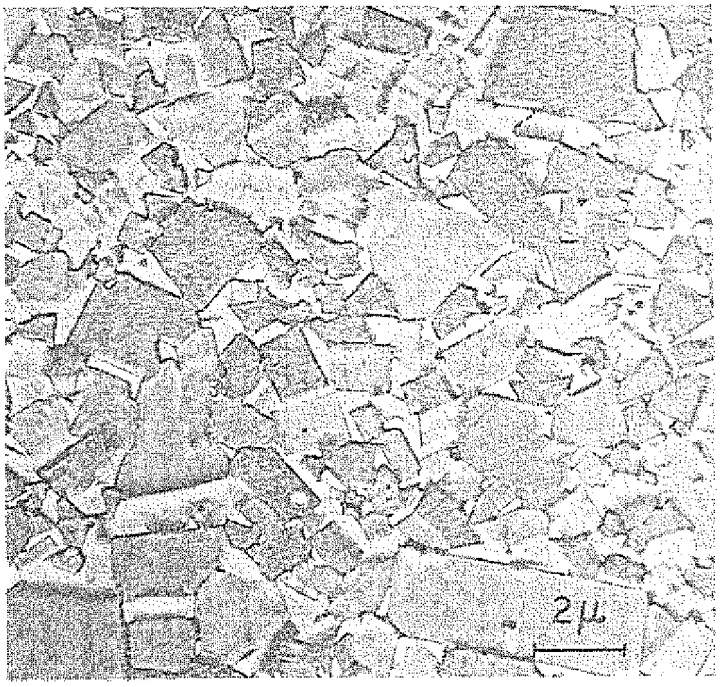

FIG. 5—*Continued.* (b) *4% cobalt by weight.*

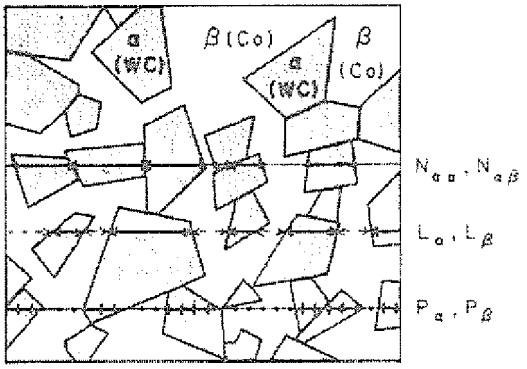

FIG. 6—*Schematic illustration of point counting* (P_α, P_β), *intercept counting* ($N_{\alpha\alpha}$, $N_{\alpha\beta}$), *and linear intercept lengths* (L_α, L_β).

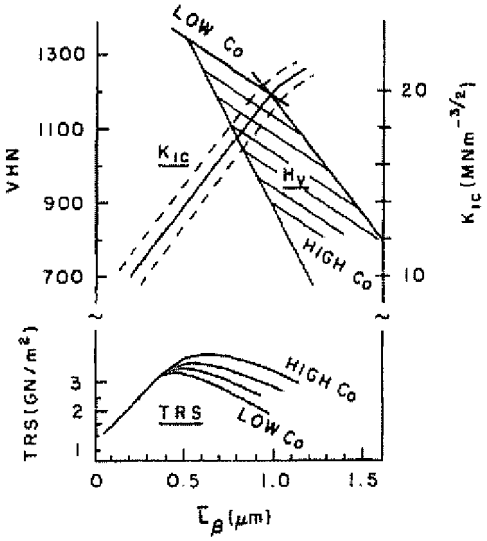

FIG. 7—*Schematic diagram showing trends of transverse rupture strength (TRS), indentation hardness (VHN), and fracture toughness, (K_{Ic}), as a function of the binder mean free path, (L_β) (after Ref 9 and Footnote 3).*

rupture strength versus mean free path curve reflects a transition between brittle and ductile fracture initiation. On the left side, the fracture strength is controlled by the largest defects and the fracture propagation resistance of the material. On the right side, fracture is associated with plastic deformation and crack nucleation at WC particles, and therefore the fracture strength is related to the yield strength. The inverse relationship between hardness and fracture strength in the brittle grades lies at the root of the basic quandary of alloy design. The carbide manufacturers and users are continuously striving for the optimum compromise between maximum hardness and adequate fracture strength.

Very little is known about the effects of contiguity as an independent variable. A tentative interpretation [*9*] of the data available appears to show that there is increasing hardness [*10*] and decreasing transverse rupture strength [*11*] with increasing contiguity. A practical difficulty is that of separating the effects of contiguity from those of the other variables contained in Eq 7.

Microscopy Applied to Research Problems

The apparent simplicity of the microstructures of cemented carbides may be misleading in suggesting that the obvious microstructural parameters (binder volume fraction, binder mean free path, and carbide grain size) exert

exclusive control over the mechanical properties. It has become painfully apparent, as the result of recent and current research, that neither is the structure quite as simple as it looks in the light microscope or in the electron microscope at moderate magnifications, nor is it always possible to predict precisely the properties of a phase mixture, such as WC-Co, even if the structure could be regarded as consisting only of hard WC particles embedded in a ductile binder matrix.

For these reasons, much of the current basic research on cemented carbides is concerned with the development of the microstructure during sintering, the deformation processes at the microstructural level, and the relation between structure and properties. Some aspects of these research topics are briefly discussed in this section.

Stereology of Multiphase Materials Applied to Cemented Carbides

Simple cemented carbides, such as WC-Co, belong to the general class of two-phase alloys or phase mixtures of coarse microstructure. Other examples of this class of alloys are dual-phase steels (ferrite-martensite), cast aluminum/silicon (Al-Si) alloys and dual-phase copper/aluminum (Cu-Al) alloys (α-β), among others. The study of the interrelationships between the microstructure and properties of phase mixtures requires stipulation of the relevant microstructural parameters. For instance, in order to consider the effects of second-phase particles on such field properties of a material as the thermal and electrical conductivity, dielectric constant, and magnetic permeability, Ondracek [*12*] identifies five parameters required to define the microstructure: (1) the number of phases implicitly present, (2) a factor relating to the geometrical arrangement of the added phase, that is, the connectivity, and (3) the concentration, (4) shape, (5) orientation of the particles. Together with the properties of the individual phases, these microstructural parameters allow calculation of the upper and lower bounds of a field property as a function of the composition of the mixture. The extreme limits of the properties of the mixture are those corresponding to the parallel and series arrays, respectively, of the phases. Closer bounds are obtained if the parameters are more precisely defined and correspond better to the geometry of the actual structure. Similar considerations apply to linear elastic properties. Closely spaced upper and lower bounds have been calculated for the elastic modulus of phase mixtures [*13,14*] and, as a matter of fact, with first application to WC-Co alloys (Fig. 8).

The theory of nonlinear mechanical behavior of phase mixtures is not nearly as well developed. The plasticity of coarse-grained two-phase alloys has been reviewed by Fischmeister and Karlsson [*15*], including the limited work done on WC-Co alloys. References to, and discussion of, the influences of microstructural features on properties are found in Exner's survey paper [*1*], with particular attention to hardness, transverse rupture strength, and fracture toughness. In general, the dominant microstructural variable in both empiri-

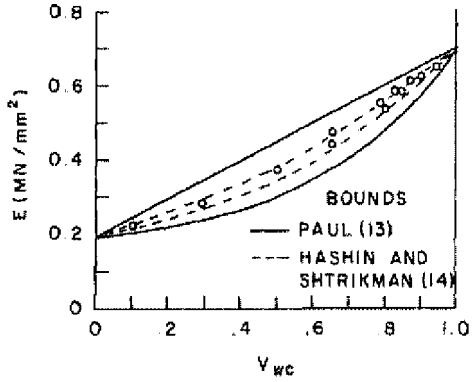

FIG. 8—*Schematic diagram of upper and lower bounds of the elastic modulus, (E), of WC-Co as a function of the volume fraction of WC [$V_{WC} = (V_V)_\alpha$] (after Fischmeister and Karlsson [15]).*

cal correlations and theoretical models is the binder mean free path, but the prediction of the strength properties from first principles requires a deeper understanding of the deformation mechanisms than is now available and further identification of the relevant microstructural features and variables. Some of the important factors are being revealed by current research, in particular the use of fractography in studying deformation and failure mechanisms and the application of transmission electron microscopy (TEM) to the fine details of the microstructure.

Quantitative Fractography

Detailed study of the fracture surface reveals the contribution of the various features of the microstructure to the fracture process. Luyckx [*16*] and Almond and Roebuck [*17*] called attention to the role of defects, such as pores, inclusions, or large WC grains, which in some cases can be located and identified on the fracture surface. The presence of defects of various sizes may account for the observed scatter of fracture strengths in bending of the more brittle alloy grades [*17,18*].

The local microstructural fracture processes in WC-Co observed on the fracture surface are (1) transgranular cleavage fracture of WC grains, (2) WC grain boundary fracture, (3) WC/cobalt interface decohesion, and (4) rupture of the binder (cobalt) ligaments (Fig. 9) [*19,20*].[3] Quantitative measurements of the lengths of fracture segments in each phase have been carried out (Fig. 10) [*19,20*].

[3] Pickens, J. R. and Gurland, J., *Materials Science and Engineering*, Vol. 33, 1978, pp. 135–142.

The plastic deformation of the binder has been studied in some detail on fracture surfaces of WC-Co [*19*]. In addition, the relative areas of the fracture surface occupied by the various microstructural types of fracture were determined by quantitative metallographic methods applied through scanning electron microscopy (SEM) and replica techniques [*21*], and the area fraction of the binder phase on the fracture surface was measured by Auger electron spectroscopy [*22*] and ion spectroscopy [*23*]. In general, it has been shown that the binder area fraction on the fracture surface is appreciably larger than the area fraction of the binder phase on a random planar section. These findings are in agreement with and relevant to the major role that the plastic deformation and ductile rupture of the binder is believed to have in the fracture process. However, fractography has also shown that the properties of the interfaces between carbide and binder, and between carbide grains, may have considerable influence on the fracture sequence and, perhaps, on the fracture strength.

Fine Structure of Sintered WC-Co by TEM

The electron microscope has exposed details of the microstructure which could not have been seen by light microscopy, with the most interesting results obtained by transmission electron microscopy (TEM) of thin films prepared by electrolytic etching or, preferentially, by ion milling. For instance, it has been shown by TEM that WC may contain a complex dislocation network structure, the nature of which is affected by deformation [*24–27*], and that the room temperature crystal structure of the binder is mostly face-centered cubic (fcc) with a high density of hexagonal close-packed (hcp) stacking faults arising during deformation [*25*].

Some attention is currently focused on the structure of the grain boundaries between WC particles in the sintered alloys. Using scanning transmission electron microscope (STEM) analysis, Sharma et al [*28*] have shown that the cobalt/tungsten atomic ratio is more than three times larger in the grain boundaries than in the grain interior. They interpret their results as providing evidence for the presence of a thin film of cobalt (~ 20Å) in the grain boundaries, thereby reopening the old controversy over whether WC forms a continuous skeleton or whether each WC grain is separated from its neighbors by a continuous cobalt film.

There is strong evidence that at least some of the grain boundaries provide a direct transition between contiguous WC crystals. Hagège et al [*29*], using TEM, observed and analyzed in detail the structure of one particular grain boundary with relatively good coincidence of the two crystals' lattices, although the grains were rotated by 90° approximately relative to each other across a common prismatic boundary plane. A small mismatch of low-index atomic planes and an additional small twist component were accommodated

FIG. 9—*Illustration of local fracture processes in WC-Co: (top) transgranular cleavage of a large WC grain in 6% cobalt alloy, replica TEM, ×13 000 (photomicroscopy by J. Pickens); (bottom) WC/WC grain boundary decohesion, showing a WC face with ruptured cobalt ligaments. SEM, ×10 000 (photomicroscopy by J. Hong.)*

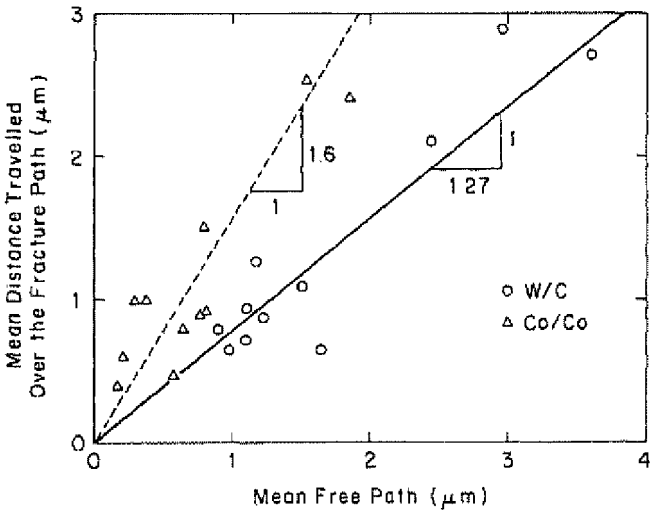

FIG. 10—*Mean fracture segment lengths in carbide (W/C) and in binder (Co/Co) as a function of mean free path [19].*

by the defect structure in the grain boundary. These results are not compatible with the presence of a cobalt film in the boundary.

The distribution of dihedral contact angles between contiguous WC grains, measured by Gurland [*30*] and Deshmukh and Gurland,[4] show pronounced peaks at 60° and 90° (Fig. 11). Such results appear to indicate a geometrical influence on the contact configuration, although they do not necessarily prove a tendency towards a unique preferred orientation across contact planes. Dihedral angles of contact measured in cubic carbide/binder systems [*31*] are a function of the relative values of the carbide/binder interface energy and carbide/carbide grain boundary energy and are generally independent of orientation.

The structure and properties of the WC grain boundaries may well be important factors in the deformation and fracture processes. Reference is made in the literature to a number of observations regarding the role of these boundaries in transmitting plastic deformation through the WC skeleton [*32,33*] and providing primary sites of crack initiation and propagation [*19–22,34*].

General Conclusions and Remarks

The producers and users of cemented carbides have greatly benefited from the development of quantitative microscopy. It is employed at all levels of ob-

[4] Work in progress.

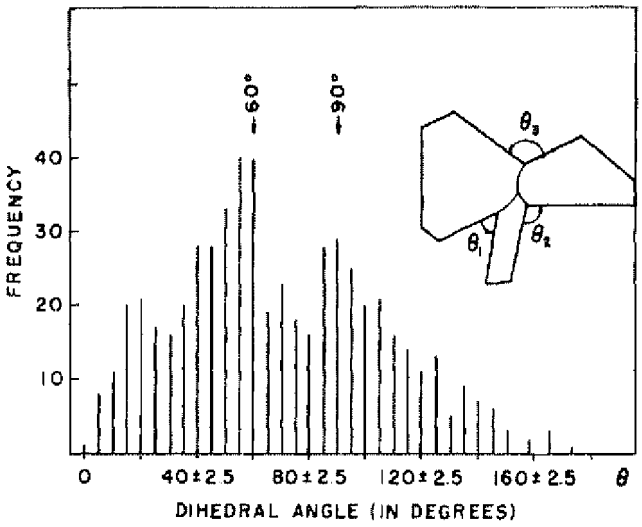

FIG. 11—*Dihedral angles between WC grains, WC-25Co, sintered ½ h at 1450°C in hydrogen (after Deshmukh and Gurland, from work in progress).*

servation, from the counting of pores at ×100, to the measurement of grain size at ×2000 and the examination of stacking faults at ×10 000. It is used for quality evaluation, alloy development, and research. The benefits are greatly improved and consistent grades of carbides.

The current trend in quality control is towards automation of inspection methods, including microscopy. In research, the recent past has seen the application of sophisticated scanning and diffraction instruments to progressively smaller features of the microstructure, and, no doubt, this trend will continue in the near future.

As a final note, it might be mentioned that an initial interest in the specific metallography of cemented carbides has more than once spawned a lasting and fruitful association between that field and the field of stereology at large, as seen, for example, in the contributions of Exner [*1,4,9*], Fischmeister [*4,15*], Chermant [*20,21*], and their co-workers to both the metallography of cemented carbides and theoretical stereology. In that sense, one can expect that the cemented carbides will continue to be a proving ground for further stereological advances.

Acknowledgment

The writing of this review was supported by the Materials Research Laboratory, funded at Brown University by the U.S. National Science Foundation.

References

[1] Exner, H. E., "Qualitative and Quantitative Interpretation of Microstructures in Cemented Carbides," *Science of Hard Materials*, Plenum Press, New York, 1983, pp. 233–262.
[2] Cherniavsky, K. S., "Stereological Methods in Studying the Cemented Carbides," *Contemporary Stereology, Stereologia Jugoslavica*, Vol. 3, Supplement 1, 1981, pp. 299–308.
[3] Gurland, J., *Transactions of the A.I.M.E.*, Vol. 200, 1954, pp. 285–290.
[4] Exner, H. E. and Fischmeister, H. F., *Archiv für Eisenhuettenwesen*, Vol. 37, 1966, p. 410.
[5] Peter, W., Kohlhaas, E., and Fischer, A., *Praktische Metallographie*, Vol. 5, 1968, p. 115.
[6] Underwood, E. E., *Quantitative Stereology*, Addison Wesley, Reading, Mass., 1970, Chapter 4.
[7] Nidikorn, B. and Davies, T. J., *Planseeberichte für Pulvermetallurgie*, Vol. 28, 1980, pp. 29–38.
[8] Werlefors, T. and Eskilsson, C., *Metallography*, Vol. 12, 1979, p. 153.
[9] Exner, H. E. and Gurland, J., *Powder Metallurgy*, Vol. 13, 1970, p. 13.
[10] Lee, H. C. and Gurland, J., *Materials Science and Engineering*, Vol. 33, 1978, pp. 125–133.
[11] Gurland, J., *Transactions of The Metallurgical Society of A.I.M.E.*, Vol. 236, 1966, p. 642.
[12] Ondracek, G., *Acta Stereologica*, Vol. 1, 1982, pp. 5–21.
[13] Paul, B., *Transactions of the A.I.M.E.*, Vol. 218, 1960, pp. 36–41.
[14] Hashin, Z. and Shtrikman, S., *Journal of the Mechanics and Physics of Solids*, Vol. 11, 1963, pp. 127–140.
[15] Fischmeister, H. and Karlsson, B., *Zeitschrift für Metallkunde*, Vol. 68, 1977, pp. 311–327.
[16] Luyckx, S. B., *Acta Metallurgica*, Vol. 23, 1979, pp. 109–115.
[17] Almond, E. A. and Roebuck, B., *Metal Science*, Vol. 11, 1977, pp. 458–461.
[18] Amberg, S. and Doxner, H., *Powder Metallurgy*, Vol. 20, 1977, No. 1, pp. 1–10.
[19] Hong, J. and Gurland, J., "A Study of the Fracture Process and Fracture Toughness of WC-Co Alloys," *Science of Hard Materials*, Plenum Press, New York, 1983, pp. 649–670.
[20] Chermant, J. L. and Osterstock, F., *Journal of Materials Science*, Vol. 11, 1976, pp. 1939–1951.
[21] Chermant, J. L., Coster, M., and Osterstock, F., *Metallography*, Vol. 9, 1976, pp. 503–523.
[22] Viswanadham, R. K., Sun, T. S., Drake, E. F., and Peck, J. A., *Journal of Materials Science*, Vol. 16, 1981, pp. 1029–1038.
[23] Otsuki, E. and Masudo, Y., *Nippon Kinzoku Gakkaishi*, Vol. 44, 1980, No. 2, pp. 117–123.
[24] Johannesson, T. and Lehtinen, B., *Physica Status Solidi (B)*, Vol. 16, 1973, pp. 615–622.
[25] Sarin, V. K. and Johannesson, T., *Metal Science*, Vol. 9, 1979, pp. 472–476.
[26] Gottschall, R. J., Williams, W. S., and Ward, I. D., *Philosophical Magazine A*, Vol. 41, 1980, pp. 1–7.
[27] Hagège, S., Vicens, J., Nonet, G., and Delavignette, P., *Physica Status Solidi (A)*, Vol. 61, 1980, pp. 675–687.
[28] Sharma, N. K., Ward, I. D., Fraser, H. L., and Williams, W. S., *Journal of the American Ceramic Society*, Vol. 63, 1979, pp. 194–196.
[29] Hagège, S., Nonet, G., and Delavignette, P., *Physica Status Solidi (A)*, Vol. 61, 1980, pp. 97–107.
[30] Gurland, J., *Metallography*, Vol. 10, 1977, p. 461.
[31] Warren, R. and Waldron, M. B., *Powder Metallurgy*, Vol. 15, 1972, pp. 166–201.
[32] Arndt, R., *Zeitschrift für Metallkunde*, Vol. 63, 1972, pp. 274–280.
[33] Liu, H. C. and Gurland, J., *Materials Science and Engineering*, Vol. 33, 1978, pp. 125–133.
[34] Luyckx, S., "Contiguity and the Fracture Process of WC-Co Alloys," *Proceedings*, Fifth International Conference on Fracture, Cannes, France, 1981, D. Francois, Ed., Pergamon Press, New York.